Flame front behaviour in a stratified iso-octane/air turbulent V-flame

Vena, P. C.; Deschamps, B.; Smallwood, G. J.; Johnson, M. R.

Proceedings of Combustion Institute, Canadian Section Spring Technical Meeting, 2010

Proceedings of Combustion Institute – Canadian Section
Spring Technical Meeting
Carleton University, Ottawa
May 9-12, 2010

Flame Front Behaviour in a Stratified Iso-Octane/Air Turbulent V-Flame

P.C. Vena [a], B. Deschamps [a], G.J. Smallwood [b], M.R. Johnson[a,*]

[a] *Mechanical and Aerospace Engineering, Carleton University, Ottawa, Canada*
[b] *Institute for Chemical Process & Environmental Tech., National Research Council of Canada*

1. Introduction

As stratified charge engines and gas turbines continue to develop, much focus has been placed on partial premixing as an optimization tool. With reductions in fuel consumption [1-3] and pollutant emissions [1,3,4], several studies have attempted to gain a greater understanding of the physical mechanisms responsible for such increases in overall combustion efficiency. However, the development of a well defined methodology that may quantify the effects of stratification, is a significant experimental challenge because of the inherent complexity of turbulent, partially premixed flames. If accurate physical models are to be developed, an experimental database is necessary to validate the results obtained through numerical predictions [5].

The effects of stratification on flames have been considered in terms of the effects of small-scale variations in mixture strength, defined in terms of local inhomogeneities [6,7], or of larger-scale variations associated with gradients in equivalence ratio [5,8-14]. Furthermore, Samson [15], Renou *et al.* [16], Robin *et al.* [17], and Garido-López and Sarkar [18] have attempted to define how these effects may be coupled to those of turbulence. Despite some conflicting results, it has been proposed that adjacent flamelets of different mixture strengths can interact, potentially altering their expected behaviour predicted solely from reactant properties. Robin *et al.* [17] suggest that the three most notable effects of stratification are: (1) the extension of the lower flammability limit, (2) the change in flame structure and topology, and (3) the variation in reaction rate.

Much of the difficulty in understanding the effects of partial premixing arises because it is generally quite challenging to separate potential effects of stratification from those of mixture strength in experimental flame configurations. In the present work, a unique approach was used to investigate topology of turbulent iso-octane/air V-flames over a range in equivalence ratios that was constant among flame conditions, allowing specific effects of large-scale equivalence ratio gradients to be evaluated. Through analysis of the results using an equivalent windowing technique to fix the range of mixture strengths for each gradient condition, the effects of large-scale equivalence ratio gradients on local front behaviour is described.

2. Experimental setup

Figure 1 shows a 63 mm x 15 mm rectangular exit burner that permits a controlled variation of local equivalence ratio along the y-axis (longitudinal axis) of the burner. The burner consists of three main sections; a 16 mm high lower section (section 1) in which two fully premixed reactant streams of mixture strengths ϕ_1 and ϕ_2 enter, two lateral mixing sections (2a,b) that consist of six (2b) and seven (2b) equally spaced and offset 10 mm wide, 152.4 m long channels filled with 3 mm diameter glass beads, and an exit section (3) where the flow is allowed to mix freely in both the longitudinal and lateral directions to produce a smoothly varying gradient in equivalence ratio. For a more detailed description of the burner and flow control system please refer to Vena *et al.* [19].

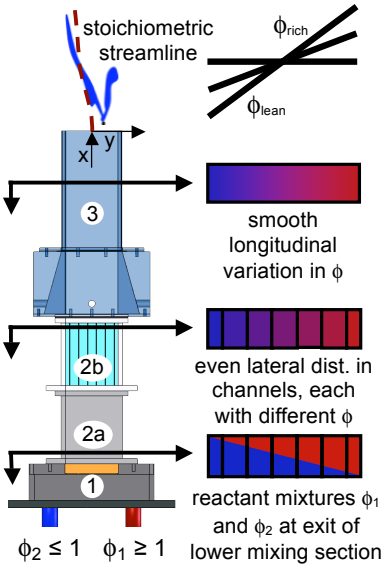

Figure 1: Mixture strength progression through lower (1), lateral (2a,b), and longitudinal (3) mixing sections

The flame was stabilized in a V-configuration with a 1.5 mm diameter rod placed perpendicular to the flow direction 5 mm downstream of the exit plane at y = 16 mm. A continuous stratified flame front thus intersected the stoichiometric streamline. Five flame conditions were evaluated by varying the equivalence ratio from 1 to 1.8 on the rich end of the burner and 1 to 0.2 on the lean end, with equivalence ratio steps of 0.2.

OH (hydroxyl) and CH_2O (formaldehyde) planar laser induced fluorescence (PLIF) was used for flow visualization to obtain instantaneous flame front topology measurements. 3-pentanone ($C_2H_5COC_2H_5$) tracer PLIF was used for qualitative equivalence ratio measurements at the exit of the burner and to indentify the stoichiometric streamline, critical to the windowing technique presented here. Figure 2 shows the laser diagnostic setup for simultaneous OH and CH_2O PLIF, which consists of a dual head Nd:YAG laser (Quanta Ray PIV-400), and Rhodamine-B dye-laser (Sirah Precision Scan),

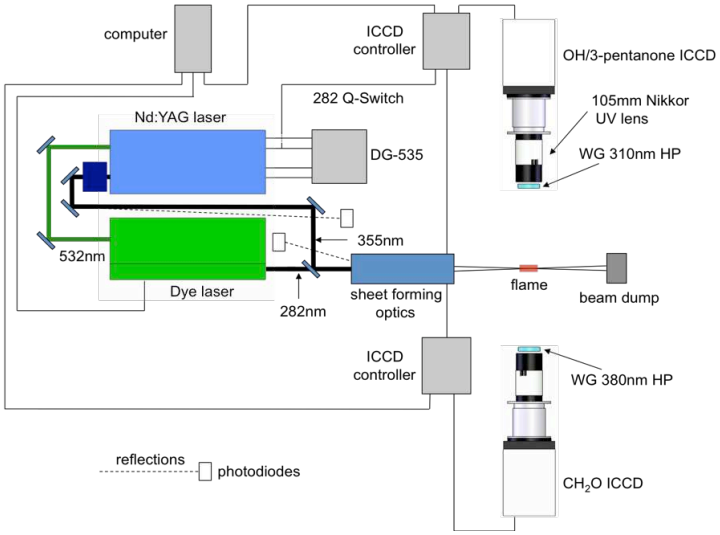

Figure 2 PLIF setup for simultaneous OH and CH_2O acquisition

A pair of PIMAX 1030 x 1034 pixel intensified cameras was used to acquire fluorescence images with a projected spatial resolution of 65 µm/pixel. This equated to an effective field of view within the flame of 32.5 mm by 67.2 mm for 3-pentanone and 48.1 mm by 67.2 mm for OH and CH_2O. For a more detailed description of the PLIF setup, please refer to Vena *et al.* [19].

2.1 Reactant Characterisation

The gradients in equivalence ratio were characterized under non-reacting conditions for all flow settings using 3-pentanone tracer PLIF by seeding the iso-octane at 7 % by volume. 3-pentanone is often used for quantitative air/fuel ratio measurements [e.g. 20,21] because of its comparable vapour properties to those of iso-octane and because its fluorescence signal is linearly dependant on concentration and laser intensity [22].. Ten images with 100 gates per exposure were acquired for each flow condition. The mean images were corrected for background and subjected to a 3x3 median filter. The individual profiles in Figure 3 were obtained by summing the rows of the corrected images corresponding to axial positions x = 0.20-0.85 mm above the exit of the burner. The five different gradient profiles are all very smooth and intersect neatly at the stoichiometric streamline where $\phi \approx 1$. Thus, by designing the experiments to track the location of this stoichiometric streamline, it was possible to isolate and observe any equivalence ratio gradient effects on flame behaviour. Furthermore, with the mean exit velocity of the burner fixed for all cases, the mean flow field and turbulence characteristics were also consistent within the region of interest (ROI) of the flame. The technique used to precisely define the region of interest is explained in detail below.

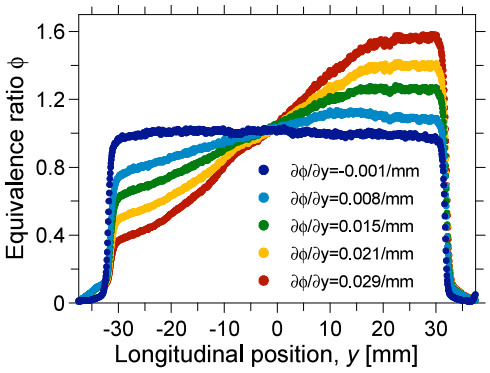

Figure 3. Longitudinal variation in equivalence ratio for five flame conditions

2.2 Flow divergence Characterisation

The stoichiometric streamline was identified under reacting conditions for each of the four stratified settings with 3-pentanone tracer PLIF. One thousand individual images were acquired at axial positions x= 2.0–34.5 mm, x= 34.5–67.0 mm, and x= 67.0-99.5 mm. Although the current setup did not simultaneously account for pulse-to-pulse variations in laser intensity, the long term stability of the laser permitted semi-quantitative measurements of average mixture strength in the unburnt gases. The individual PLIF images were corrected for both background intensity and laser profile variations. After generating an ensemble average image, a 3 x 3 pixel (0.19 mm x 0.19 mm) median filter was applied to eliminate any residual shot noise. The resultant image was then conditioned on reactants using a map of the reactant progress variable derived from an ensemble average of a binarized version of the same 3-pentanone images. Continuous maps of reactant 3-pentanone concentrations, generated by combining image sets from the three different heights, were used to evaluate the local mixture strength within the reactants up to approximately 10 cm above the burner exit nozzle. A sample final reactant concentration image for $\partial\phi/\partial y = 0.021/\text{mm}$ is shown in Figure 4.

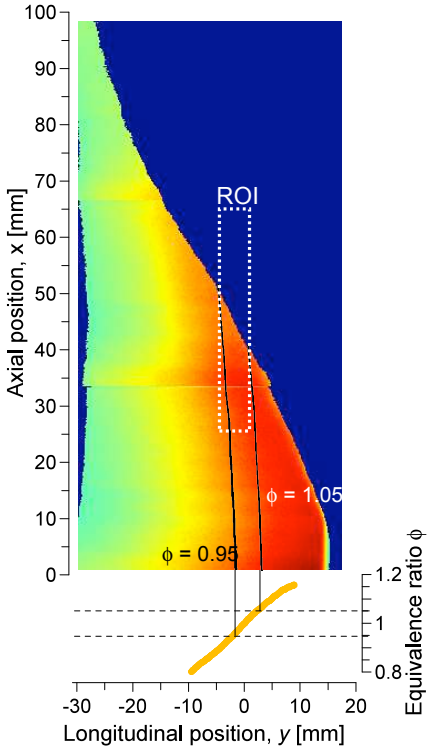

Figure 4 Mixture strength distribution and corresponding interrogation window for partially-premixed flame setting $\partial\phi/\partial y = 0.021/\text{mm}$

Concentration images were derived for all stratified flame conditions and were used to identify the location of the stoichiometric streamline as well as the average mixture strength at the mean position of the flame front, $\langle c \rangle = 0.5$, within the turbulent flame brush. To ensure fair comparison between different flame settings and to isolate the effects of mixture gradients from those of local mixture strength, it was necessary to maintain a constant range of equivalence ratios within the analysis region of the flame. This was accomplished by varying the width of the region of flame being analyzed, highlighted as the superimposed dashed white box in Figure 4. The width of this box was precisely adjusted for different flame conditions to keep the range of equivalence ratios it contained constant between $0.95 \le \phi \le 1.05$ for all flames. Figure 4 also shows the corresponding $\phi = 0.95$ and $\phi = 1.05$ streamlines used to define the interrogation region for the $\partial\phi/\partial y = 0.021/\mathrm{mm}$ flame. By carefully specifying the widths of these analysis regions, it was possible to assume the flames within were propagating under essentially identical mean flow and equivalence ratio conditions, while being subjected to widely differing gradients.

3. Results and Discussion

One thousand individual OH and CH_2O PLIF images were acquired for each of the five flame settings. The CH_2O images were spatially matched to the OH images using a 90 point target to ensure that corresponding pixels of each camera imaged identical positions within the flame. Images were background and laser profile corrected, and subjected to a 3x3 median filter to reduce shot noise. Images were studied to quantify the effect of gradient on turbulent brush thickness and orientation, flame surface density, and curvature.

Within the interrogation region of each flame condition, the PDF of the magnitude of the local fluctuations in equivalence ratio, or small-scale inhomogeneities, was determined for the reactant mixture and was revealed to be comparable for all flame settings. This implied that both the distribution and size of the small-scale spatial variations in ϕ, shown to affect flame properties by Jiménez *et al.* [23], were constant for all test conditions. Therefore, any observed differences in flame properties could be attributed to large-scale gradient effects.

3.1 Flame Surface Density

Two dimensional flame surface density (FSD) data were calculated following the approach proposed by Deschamps *et al.* [24] where Σ is derived from the definition of Pope [25], $\Sigma = \langle \Sigma' \rangle = \left\langle |\nabla c| \cdot \delta\left(c - c_f\right) \right\rangle$, for which $|\nabla c|$ is the absolute value of the spatial flame front gradient, $\delta\left(c - c_f\right)$ is the instantaneous flame position, and δ is the Kronecker delta. The instantaneous FSD, Σ', was obtained from flame contours derived from individual binarized OH PLIF images with the position of the flame front determined by thresholding. Any noise originating from the false fronts was effectively removed by multiplying the instantaneous Σ' images with the matching binary CH_2O PLIF image. This approach was derived from the method of Paul and Najm [26] for heat release rate calculations. Briefly, they determined that the product of OH and CH_2O was a better approximation of the position of the flame front than OH. Results were plotted in terms of $\langle c \rangle$ for cases where the analysis window spanned the entire flame front and the progress variable ranged from approximately 0 to 1.

Figure 6 shows the slightly skewed FSD profiles with maximum values in the vicinity of $\langle c \rangle = 0.6$, consistently falling toward the burnt gases. The asymmetric profiles were consistent with those of turbulent V-flames observed by Shepherd [27] for premixed methane/air and ethylene/air, and Anselmo-Filho *et al.* [5] for partially-premixed methane/air mixtures. This implies that the $k\langle c \rangle\left(1 - \langle c \rangle\right)$ expression, used for chemical closure models for fractal flamelets [28], does not provided a good estimate of $\Sigma\left(\langle c \rangle\right)$ for the current data. It was proposed by Shepherd [27] that the ordered, cusped structure of the V-flame, contributes to the asymmetry in FSD. This was confirmed by their observation of bimodal PDFs of flame orientation [27].

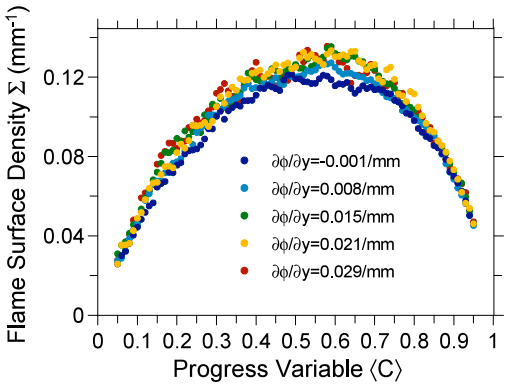

Figure 6 Flame Surface Density of OH for premixed and stratified flames

Although the bias of the FSD profiles did not vary among conditions, comparing the homogeneous and stratified profiles reveals a non-linear increase in FSD with increasing gradient. The effect is strongest for the weaker gradients but levels off as stratification increases. This was expected based on the qualitative visual inspection of individual fluorescence images, in which stronger mixture gradients were associated with increased wrinkling and corrugation of the flame front, ultimately leading to the appearance of local extinctions along the stratified front. The appearance of extinctions explains the levelling off of FSD for the largest mixture gradients. Although the measured flame brush thickness (defined as the perpendicular distance between $\langle c \rangle$=0.1 and $\langle c \rangle$=0.9 contours) was consistently greater with stratification (~10.5 mm compared to 9.5 mm for the homogeneous flame at the same axial position x = 45 mm above the exit of the burner), it did not change significantly as the gradient was increased. This suggests that the dominant effect of large scale mixture gradients may be to enhance both the number and intensity of wrinkles, similar to the reported effects of small scale inhomogeneities in equivalence ratio [6,7].

3.2 Curvature

Figure 7 shows the length-weighted PDFs for each flame setting, calculated by normalizing the number of observations in each bin by the total number of local curvature measurements. Although the curvature PDFs were nearly symmetrical, a slight bias toward the reactants was observed. This is consistent with the FSD results of Figure 6, and the generally accepted trend for cusped flame fronts, where the larger area of positive fronts results in the biased curvature plots. The negligible flame area of the infrequent cusps, manifested as large negative curvatures [29], further emphasize the shift towards the reactants.

The maximum curvature was consistently around 0.2 mm^{-1} and the probability of encountering this level of curvature decreased only slightly for stronger gradients, contrary to the observations of Anselmo-Filho *et al.* [5] who reported a change in bias with gradient. Furthermore, no significant increase in variance with stratification was observed in the present results.

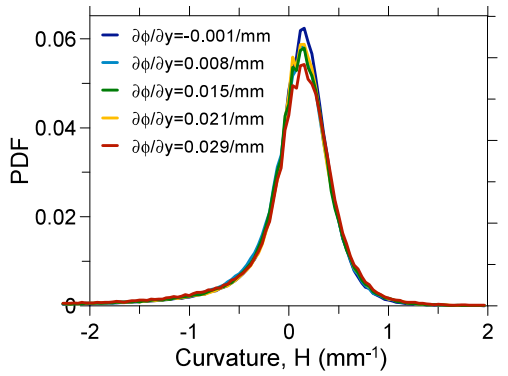

Figure 7 Comparison of curvature PDFs for globally stoichiometric premixed and partially-premixed iso-octane/air V-flames

The apparent discrepancy between the present topology results and those of Anselmo-Filho *et al.* [5] for globally lean methane/air flames can arguably be attributed to differences in mixture strength, methodology, and fuel type. Firstly, as suggested by Zhou *et al.* [6] stratification has a greater effect on flame propagation for off-stoichiometric mixtures, with the inherent thermo-diffusive stability of stoichiometric flames limiting the effects of stratification. Secondly, the variable interrogation windowing technique used in the present analysis to freeze the range of equivalence ratios (and hence Lewis numbers) may at least partially affect the interpretation of flame topology variations. Finally, because of the significant difference in the Markstein numbers for iso-octane/air versus methane/air flames [30], it is reasonable to expect that the response to perturbations from the stabilizing rod could be different in the two cases, again affecting the significance or magnitude of observed differences in flame topology with increased mixture gradient.

4. Conclusion

The effects of mixture gradients on the topology of a turbulent V-flame were studied with PLIF images of OH and CH_2O. A unique windowing approach was presented that ensured the range in equivalence ratios within the interrogation region of the flame was kept constant for all flame settings, thus isolating the effect of large-scale gradients from that of local inhomogeneities on flame propagation. Although qualitative visual inspection of the images showed significant changes in front wrinkling, and suggested the presence of local extinctions, the quantitative increase in flame surface density was more modest. It was thus proposed that the resulting decrease in flame length brought about by the onset of local extinctions balanced the increase in FSD. Furthermore, the curvature pdfs revealed negligible effects of gradient, contrary to those reported in the literature for lean methane/air flames, suggesting that the thermodiffusive stability of stoichiometric flames may help attenuate large-scale gradient effects.

REFERENCES

[1] Y. Takagi, Proc. Combust. Inst. 27 (1998) 2055-2068.
[2] S. Shiga *et al.*, Combust. Flame 129 (1-2) (2002) 1-10.
[3] F. Zhao, M.C. Lai, D.L. Harrington, Progress in Energy and Combust. Science 25 (1999) 437–562.
[4] C. Poppe, S. Sivasegaram, J.H. Whitelaw, Control of NO_x Emissions in Confined Flames by Oscillations, Report No. TF/96/09, Imperial College, London, England.
[5] P. Anselmo-Filho, R.S. Cant, S. Hochgreb, R.S. Barlow, Proc. Combust. Inst. 32 (2009) 1763-1770.
[6] J. Zhou, K. Nishida, T. Yoshikazi, H. Hiroyasu, SAE technical series (1998) paper no. 982563.
[7] Y.-S. Cho, D.A. Santavicca, SAE technical series (1993) paper no. 932715.
[8] Y. Ra, W.K. Cheng, The Fifth Int'l Sym on Diag and Mod of Comb in Internal Comb Engines (2001) 251-257.
[9] T. Kang, D.C. Kyritsis, Combust. Sci. and Tech. 177 (2005) 2191-2210.
[10] T. Kang, D.C. Kyritsis, Energy Conversion and Management 48 (2007) 2769-2774.
[11] T. Kang, D.C. Kyritsis, Proc. Combust. Inst. 32 (2009) 979-985.
[12] Y.M. Marzouk, *et al.*, Proc. Combust. Inst. 28 (2000) 1859-1866.
[13] A. Pires Da Cruz, A.M. Dean, J.M. Grenda, Proc. Combust. Inst. 28 (2000) 1925-1932.
[14] N. Pasquier, *et al.*, Proc. Combust. Inst. 31 (2007) 1567-1574.
[15] E. Samson, PhD thesis, Institue National des Sciences Appliquées de Rouen, France, 2002.
[16] B. Renou, E. Samson, A. Boukhalfa, Combust. Sci. and Tech. 176 (2004) 1864-1890.
[17] V. Robin, *et al.*, Combust. Flame 153 (2008), 288-315.
[18] D. Garido-López, S. Sarkar, Proc. Combust. Inst. 30 (2005) 621-628.
[19] P.C. Vena, et al., Proc. Combust. Inst. 33 (2010), PROCI-D-10-00879 (*accepted for presentation*).
[20] S. Einecke, C. Schulz, V. Sick, Appl Phys B (71) (2000), 717–23.
[21] M. Richter, B. Axelsson, K. Nyholm, M. Aldén, Proc. Combust. Inst. 27 (1998), 51-57.
[22] H. Neij, B Johanson, M. Aldén, Combust. Flamme 99 (1994) 449-457.
[23] C. Jiménez, B. Cuenot, T. J. Poinsot, D. C. Haworth, Combust. Flame 128 (2002) 1-21.
[24] B.M. Deschamps, *et al.*, Proc. Combust. Inst. 26 (1996), 427-435.
[25] S.B. Pope, Int. Journal of Engineering Science 26 (1988), 445-469.
[26] P. Paul, H. Najm, Proc. Combust. Inst. 27 (1998), 43-50.
[27] I.G. Shepherd, Proc. Combust. Inst. 26 (1996) 373-379.
[28] F.C. Gouldin, P.C. Miles, Combust. Flame 100 (1995) 202-210.
[29] T.W. Lee, G.L. North, D.A. Santavicca, Combust. Flame 93 (1993) 445-456.
[30] X.J. Gu, M.Z. Haq, M. Lawes R. Woolley, Combust. Flame 121 (2000) 41–58.